[1] **Zhongqiang Zhou**

[1] **Jianwei Ma**

[1] **Yuan Wen**

[1] **Xiaofang Liu**

[2] **Jie Zhuang**

[2,*] **Jupeng Zeng**

A High-Impedance Fault Detection and Faulty Feeder Selection Method Based on Zero Sequence Current Active Regulation Principle

JES

Journal of Electrical Systems

Abstract: - In distribution networks, the existing single-phase ground fault (SPG) protection technology faces challenges in reliably detecting high-impedance faults (HIFs). Moreover, the selection of faulty feeders is susceptible to the influence of distribution network parameters. To address these issues, a novel method for HIF detection and faulty feeder selection is proposed, which remains unaffected by asymmetrical distribution network conditions. The approach involves injecting current into the distribution network via an active inverter device. Then, a dynamic sensing criterion for ground faults is constructed based on the characteristics of the injected current and the change in zero-sequence current for each feeder. By adjusting the zero-sequence voltage, the difference between the zero-sequence currents of the faulty and healthy feeders is enhanced. Therefore, the amplitude characteristics of the zero-sequence current are then utilized to effectively identify the faulty feeder. The proposed method is validated through PSCAD/EMTDC simulation, demonstrating its capability to accurately identify HIFs and eliminate the influence of asymmetrical distribution network parameters on fault detection and faulty feeder selection.

Keywords: Asymmetrical distribution network, single-phase ground fault detection, high-impedance faults, faulty feeder detection, fault current amplification.

I. INTRODUCTION

The 10kV distribution network spans a wide area, but it faces significant challenges related to feeder faults. Single-phase grounding (SPG) faults account for up to 80% of these issues [1,2]. Additionally, the integration of distributed power supply sources complicates the network structure. One specific type of fault is HIF, which occurs frequently due to various factors such as tree barriers, feeders falling off the road, and grass interference. HIFs present unique characteristics that make them difficult to detect. The fault resistance is high, which affects the visibility of electrical quantity changes during faults [3,4]. Moreover, traditional SPG fault detection methods struggle with accuracy and sensitivity in the presence of capacitive currents from the distribution network and three-phase feeder asymmetry [5,6]. Therefore, HIFs exhibit high fault resistance, making their electrical quantity characteristics less obvious during fault conditions. Detecting HIFs promptly is crucial because they can persist for extended periods without being detected, endangering both the distribution network and personal safety [7].

The resonant grounding method has the advantages of limiting SPG current, automatically eliminating transient ground faults, and improving power supply reliability [8]. However, in resonant grounding systems in the application of normal operating conditions to avoid the capacitive current, three-phase unbalanced overvoltage caused by three-phase ground parameter imbalance, etc. on the traditional zero-sequence voltage overrun start, the field is generally used away from the resonance point of the operation of the with the adjustable type of arc-suppression coil [9]. Alternatively, pre-tuned arcing coils with damping resistors connected in series or parallel to the arcing coil are used for unbalanced overvoltage suppression [10-12]. Both methods are at the expense of the sensitivity of sensing ground faults, and when a HIF occurs in the distribution network, the neutral zero-sequence voltage may be lower than the threshold voltage for fault detection, which leads to fault protection refusal [13].

With the development of power electronics technology in recent years, the use of active inverters to flexibly change the neutral point voltage is a new method for dynamic suppression of neutral point displacement voltage in resonantly grounded distribution networks [14-16]. This type of method can dynamically adjust the injected current to suppress the neutral displacement voltage to 0 when the system parameters change, thus eliminating the unbalanced overvoltage. However, after the device is put into use, the displacement voltage is always suppressed to 0. At this time, if a single-phase grounding fault occurs, the zero-sequence voltage relay will not be able to start

according to the zero-sequence voltage overrun, which affects the timely perception and treatment of a single-phase grounding fault [17].

For the influence of distribution network parameters on SPG protection, most of the current studies mainly focus on the influence of distribution network parameters on fault phase selection, while there are fewer studies on the influence of distribution network parameters on fault feeder selection. Literature [18,19] analysed the movement trajectory of neutral point voltage when a SPG occurs in an asymmetrical distribution network. The influence of three-phase asymmetry on feeder selection was eliminated by detecting the amount of change in three-phase voltage magnitude and phase before and after the fault. However, this method requires a known compensation state of the system and is difficult to implement in the field. Literature [20] concludes that the amount of change in the three-phase current of healthy feeders is the same by analyzing the amount of change in the three-phase current of each feeder before and after the fault. Based on this, a faulty feeder selection method is constructed. Literature assumes that the three-phase load current is unchanged, but the transient process time of HIF is long, and the effect of load current on the amount of current change cannot be completely ignored. Literature [21] based on the traditional zero-sequence conductor fault feeder selection method combines the characteristic frequency zero-sequence conductor measured during the transient process with the industrial frequency zero-sequence conductor for fault feeder selection. However, the influence of distribution network parameters on the zero-sequence conductance of the feeder is not considered.

In the context of resonant grounding systems, various techniques exhibit limitations when it comes to HIFs protection. To address this, a dynamic sensing approach for ground faults is realized by utilizing the root-mean-square (RMS) value of the injected current change after a fault occurs. By regulating the zero-sequence voltage within the system, the differentiation between the zero-sequence currents of faulty and healthy feeders is enhanced. Leveraging the amplitude characteristics of the zero-sequence current, the faulty feeder can be effectively identified. To validate this method, a typical 10kV distribution network model with DG is constructed using PSCAD/EMTDC simulation software. The simulation results confirm the effectiveness of the proposed approach.

II. ANALYSIS OF SPGs IN DISTRIBUTION NETWORKS

A. The impact of DG access

To ensure the stability of the system, the neutral grounding method of the main network should be unaffected by the casting and cutting of DG. Therefore, when the main grid side is grounded by the arc-suppression coil, the high voltage side of DG should adopt the neutral point non-effective grounding method. When DG is connected to the grid, the capacitive current to the ground can be compensated through the main grid side, so DG does not need to install an arc-suppression coil. The use of a neutral non-grounding method further reduces the system cost and tuning complexity.

When the DG grid-connected side transformer adopts the $\triangle$/Y winding wiring method, the zero-sequence network of the system does not change. After a fault occurs, the current flow path between the DG and the main grid side is cut off, and the distribution of steady-state zero-sequence current in the network is not affected. Therefore, the fault feeder selection method using the steady-state zero-sequence signal is still applicable.

Inverter-type DGs are more widely used in distribution networks, and their simulation model control framework is shown in Fig. 1.
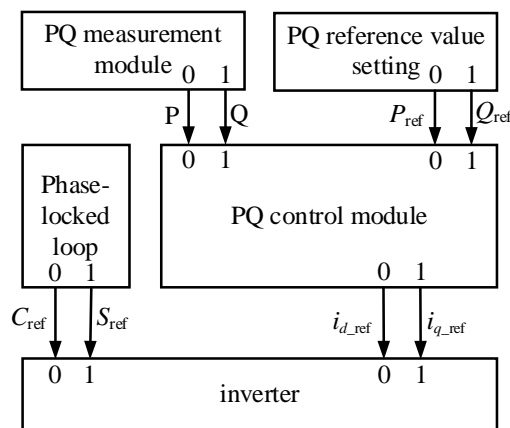
Figure 1: Grid-connected inverter control block diagram

In Fig. 1, P and Q are the active and reactive power of the inverter, respectively. P_{ref} and Q_{ref} are the reference values of active and reactive power, respectively. i_{d_ref} and i_{q_ref} are the reference values of the d-axis and q-axis components of the current, respectively. S_{ref} and C_{ref} are the reference values of the sinusoidal and cosinusoidal values of the phase angle of the voltage, respectively. The outer loop is a constant power control where the PQ measurement module is used to calculate the output power of the inverter. The active and reactive power reference values are given by the PQ reference value setting module. The PQ control module is the core of the outer loop control. The inner loop controller uses modules that come with the software.

B.   Steady-state zero-sequence current characteristics
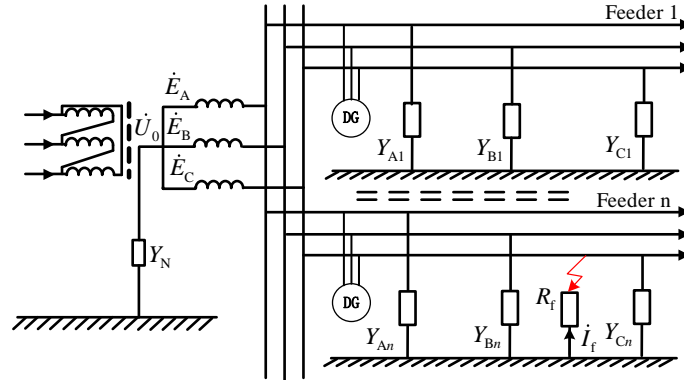
Figure 2: Schematic diagram of SPG in the distribution network

The schematic diagram of the distribution network when a SPG occurs is shown in Fig. 2. Where $\dot{E}_A$, $\dot{E}_B$ and $\dot{E}_C$ are the three-phase power supply electromotive force. $\dot{U}_0$ is the zero-sequence voltage. $Y_{X1} = g_{X1} + j\omega C_{X1}$ (X=A, B, C) is the three-phase-to-ground admittance of feeder 1. g_{X1} and C_{X1} are the three-phase zero-sequence conductance and capacitance of feeder 1, respectively. $Y_{Xn} = g_{Xn} + j\omega C_{Xn}$ (X=A, B, C) is the three-phase-to-ground admittance of feeder n. g_{Xn} and C_{Xn} the three-phase zero-sequence conductance and capacitance of feeder n. R_f is the fault resistance at the faulty point. Y_N is the neutral conductance, and $Y_N = -j\dfrac{1}{\omega L} = -j(1-v)\omega C$.

where $v = (I_C - I_L)/I_C$, which is less than 0 when the system is overcompensated. L is the arc-suppression coil inductance. C is the total zero-sequence capacitance of the distribution network. $\dot{I}_f$ is the faulty current.

i. Analysis of Factors Affecting the Characteristics of Steady-State Zero-sequence Current Amplitude and Phase Angle Faults

When a SPG occurs in phase C of the feeder n, and the fault resistance is R_f. Then, the zero-sequence current of the faulty feeder $\dot{I}_{0n}$:

$$\dot{I}_{0n} = \dot{U}_0 Y_{\Sigma n} + \dot{E}_C Y_{asy-n} - \frac{\dot{U}_0}{\dot{E}_C}\dot{I}_{f\max} \tag{1}$$

Where $Y_{\Sigma n} = Y_{An} + Y_{Bn} + Y_{Cn}$ is the total zero-sequence admittance of the feeder n; Y_{asy-n} represents the three-phase-to-ground asymmetry admittance of the feeder n:

$$Y_{asy-n} = G_A + j\omega C_A + a^2(G_B + j\omega C_B) + a(G_C + j\omega C_C) \tag{2}$$

Where $a = e^{j120}$ is the rotation factor; G_A, G_B and G_C are the three-phase-to-ground conductance; C_A, C_B, and C_C are the three-phase-to-ground capacitance.

The zero-sequence current of the healthy feeder $\dot{I}_{0i}$:

$$\dot{I}_{0i} = \dot{U}_0 Y_{\Sigma i} + \dot{E}_C Y_{asy-i} \tag{3}$$

From Eq. (1) and Eq. (2), the zero-sequence current of the faulty feeder contains three components. First, this current is the inherent zero-sequence current of the feeder $\dot{E}_{\mathrm{C}}Y_{asy-n}$ and it is not affected by the fault resistance. Next, the feeder zero-sequence conductor current generated by the feeder-to-ground conductor under the effect of the zero-sequence voltage $\dot{U}_0 Y_{\Sigma n}$, and the fault current generated by the fault resistance $\dot{U}_0 \dot{I}_{\mathrm{f\,max}}/\dot{E}_{\mathrm{C}}$. While the zero-sequence current of the healthy feeder does not contain fault current. The magnitude and phase angle of the inherent zero-sequence current are random and affect both the magnitude and phase of the zero-sequence current. In addition to the inherent zero-sequence current, all other components of the zero-sequence current decrease with the decrease of the $\dot{U}_0$ and are related to the fault resistance.

The feeder equivalent zero-sequence admittance is the ratio of the $\dot{I}_{0n}$ to the $\dot{U}_0$, then the zero-sequence admittance of the faulty feeder Y'_{0n}:

$$Y'_{0n}=Y_{\Sigma n}\left(\frac{1+Y_{\Sigma n}R_{\mathrm{f}}}{Y_{\Sigma n}R_{\mathrm{f}}}-\frac{1+\dot{K}_n Y_{\Sigma n}R_{\mathrm{f}}}{Y_{\Sigma n}R_{\mathrm{f}}}\frac{1+Y_{\mathrm{N}}R_{\mathrm{f}}+Y_{\Sigma}R_{\mathrm{f}}}{Y_{\Sigma n}\left(Y_{\Sigma}R_{\mathrm{f}}\dot{K}_{\mathrm{s}}+1\right)}\right) \tag{4}$$

where $\dot{K}_n$ is the asymmetry of the feeder n:

$$\dot{K}_n=\frac{a^2 Y_{\mathrm{A}n}+aY_{\mathrm{B}n}+Y_{\mathrm{C}n}}{Y_{\mathrm{A}n}+Y_{\mathrm{B}n}+Y_{\mathrm{C}n}} \tag{5}$$

From Eq. (4) and Eq. (5), it can be shown that the feeder asymmetry and the fault resistance affects the magnitude and phase angle of Y'_{0n}.

ii. Analysis of factors affecting steady-state zero-sequence currents
To investigate the effect of fault resistance on the zero-sequence current of the feeder, the variation of the zero-sequence current characteristics with the fault resistance is plotted based on the data in Tab. 1 and the results are shown in Fig. 3.

Table 1: Typical 10kV distribution system parameters

Parameters	Value
System capacitance current	150A
v	-15%
Distribution network and feeder damping ratio	5%
Degree of asymmetry of distribution networks and feeders	$0.035e^{j\pi/3}$
Feeder capacitance current	20A
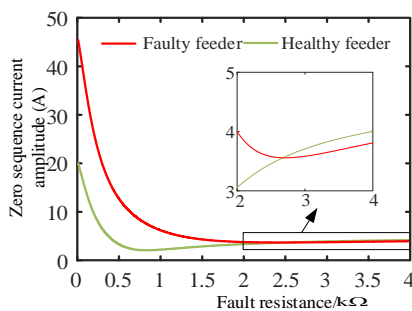
(a)Relationship between feeder zero-sequence current magnitude and fault resistance
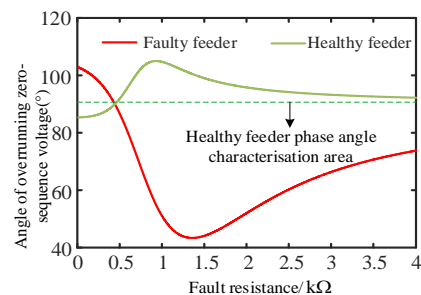
(b)Relationship between feeder zero-sequence current phase and fault resistance

Figure 3: Variation of feeder zero-sequence current with different fault resistance

From Fig. 3(a), it can be shown that the zero-sequence current is strongly influenced by the fault resistance. With the increase of fault resistance, the amplitude of the feeder zero-sequence current gradually decreases. The difference between $\dot{I}_{0\mathrm{i}}$ and $\dot{I}_{0n}$ gradually decreases, and even the situation that I_{0i} is larger than I_{0n} occurs. The fault current and the zero-sequence admittance current decrease with the increase of the fault resistance. While the

inherent zero-sequence current is not affected by the fault resistance, its effect on the zero-sequence current will be highlighted with the increase of the fault resistance. As can be shown in Fig. 3(b), when the fault resistance is above 700 Ω, the angle between $\dot{I}_{0n}$ and $\dot{U}_0$ is less than $90°$, which exhibits the characteristics of a sound feeder. And a healthy feeder due to the effect of asymmetry current aggravation, the angle of feeder zero-sequence current exceeding $\dot{U}_0$ is over $90°$, which is manifested as the characteristics of the faulty feeder. Therefore, the increase of fault resistance leads to weak zero-sequence current fault characteristics, coupled with the confusion of asymmetry components, seriously affecting the reliability of the faulty feeder selection .

From Eq. (4) and Eq. (5), it can be shown that the system feeder asymmetry affects the zero-sequence admittance of the feeder. The variation of Y'_{0n} under high resistance ground fault is shown in Fig. 4 when the degree of asymmetry of the distribution network is obtained with the variation of asymmetry of the faulty feeder with the parameters shown in Tab. 2.

Table 2: Three-phase ground conductance of distribution network and total conductance of feeder n to ground

Parameters	Value
$Y_A / \mu S$	$152.68 + j5089.38$
$Y_B / \mu S$	$152.95 + j5098.33$
$Y_C / \mu S$	$152.54 + j5084.62$
$Y_{\Sigma} / \mu S$	$452.39 + j15079.64$
Y_N / mS	$-j16.59$
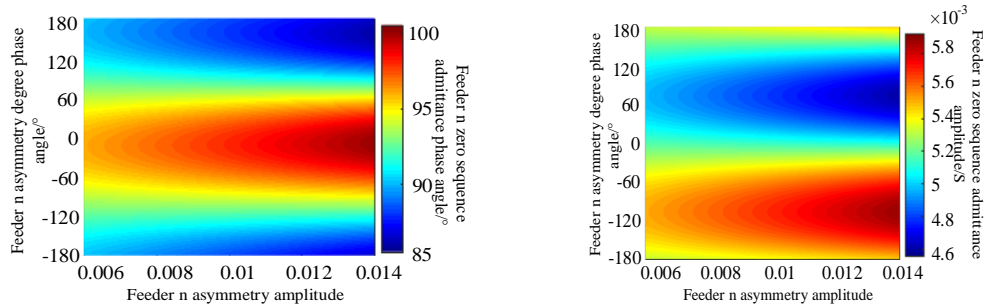
(a)Zero-sequence conductance phase angle of faulty feeder

(b)Zero-sequence conductance amplitude of faulty feeder

Figure 4: Zero-sequence admittance of faulty feeder at different symmetries

From Fig. 4, it can be shown that feeder asymmetry affects the zero-sequence admittance phase angle and magnitude after feeder failure. From Fig. 4(a), it can be shown that the feeder asymmetry degree change has a limited effect on the zero-sequence conductor phase angle after the feeder fault. As the asymmetry magnitude increases, the greater the effect of the asymmetry phase angle change on the feeder zero-sequence admittance . When the asymmetry magnitude is 0.014, the feeder asymmetry phase angle change can cause the faulty feeder zero-sequence conductance phase angle to change between $85°$ and $100°$. At this time, the faulty feeder and the healthy feeder conductor phase angle (about $87°\sim89°$) are the same, and there is a possibility of faulty feeder identification misjudgement. From Fig. 4(b), when the faulty feeder zero-sequence admittance phase angle is close to $180°$ and $0°$, the faulty feeder selection method based on the active component of the zero-sequence current will also fail at this time.

III. HIGH-IMPEDANCE FAULT DETECTION AND FAULTY FEEDER SELECTION METHOD INDEPENDENT OF DISTRIBUTION NETWORK PARAMETERS

The sensitivity and accuracy of traditional methods for HIFs detection and faulty feeder selection in distribution networks are greatly affected by the capacitive current and three-phase asymmetry of the distribution network. In this chapter, a high-resistance fault detection and fault feeder selection method that is not affected by distribution network parameters is proposed. Firstly, the principle of active intervention of injected current on $\dot{U}_0$ and $\dot{I}_0$ is explained. The characteristics of the injected current and zero-sequence current when the regulated $\dot{U}_0$ is 0 are

analyzed. According to the phenomenon that the variation of injected current is independent of system parameters when the regulated $\dot{U}_0$ is 0, the ground fault detection criterion is constructed. The faulty feeder selection method is carried out by comparing the RMS values of the zero-sequence currents of each feeder. The method is stable for HIFs detection and faulty feeder selection and is not affected by system parameters.

A.   Zero-sequence voltage and zero-sequence current active intervention principle

When the ground fault occurs in phase C of the distribution network through the fault resistance, it is shown in Fig. 5, where Y_N is the neutral point grounding admittance, g_f is the fault point fault conductance, and $\dot{I}_i$ is the zero-sequence current injected by the active inverter injection device.
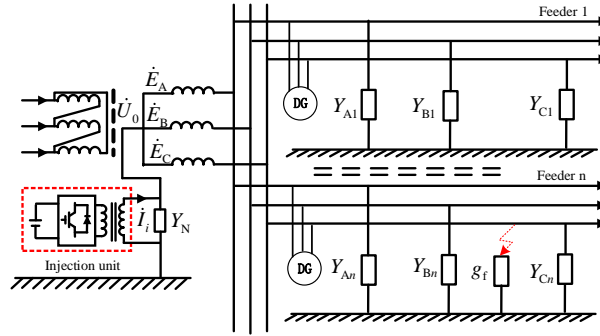
Figure 5: Schematic diagram of the C-phase-to ground fault

As shown in Fig. 5, the neutral point of the distribution network plus the active inverter injection device can be regarded as a controlled current source. The $\dot{U}_0$ and zero-sequence current of the distribution system after a fault can be solved by the superposition principle. When the active inverter injection device does not function, the neutral point voltage $\dot{U}_0'$ can be written as:

$$\dot{U}_0' = -\frac{\dot{E}_A Y_A + \dot{E}_B Y_B + \dot{E}_C \left(Y_C + g_f\right)}{Y_A + Y_B + Y_C + g_f + Y_N} \tag{6}$$

where, Y_X (X=A, B, C) are the three-phase-to-ground admittance.

The zero-sequence currents of healthy feeder $\dot{I}_{01}'$ and faulty feeder $\dot{I}_{0n}'$ are shown in :

$$\dot{I}_{01}' = \dot{E}_A Y_{A1} + \dot{E}_B Y_{B1} + \dot{E}_C Y_{C1} - \frac{\dot{E}_A Y_A + \dot{E}_B Y_B + \dot{E}_C \left(Y_C + g_f\right)}{Y_A + Y_B + Y_C + g_f + Y_N}\left(Y_{A1} + Y_{B1} + Y_{C1}\right) \tag{7}$$

$$\dot{I}_{0n}' = \dot{E}_A Y_{An} + \dot{E}_B Y_{Bn} + \dot{E}_C \left(Y_{Cn} + g_f\right) - \frac{\dot{E}_A Y_A + \dot{E}_B Y_B + \dot{E}_C \left(Y_C + g_f\right)}{Y_A + Y_B + Y_C + g_f + Y_N}\left(Y_{An} + Y_{Bn} + Y_{Cn} + g_f\right) \tag{8}$$

The fault current $\dot{I}_f'$ can be written as :

$$\dot{I}_f' = \dot{E}_C g_f - \frac{g_f \left[\dot{E}_A Y_A + \dot{E}_B Y_B + \dot{E}_C \left(Y_C + g_f\right)\right]}{Y_A + Y_B + Y_C + g_f + Y_N} \tag{9}$$

When the active inverter injection device acts alone, the power supply of the distribution system is equivalent to a short circuit. The neutral voltage $\dot{U}_0''$ can be written as:

$$\dot{U}_0'' = \frac{\dot{I}_i}{\left(Y_N + Y_A + Y_B + Y_C + g_f\right)} \tag{10}$$

The zero-sequence currents of healthy feeder $\dot{I}_{01}''$ and faulty feeder $\dot{I}_{0n}''$ are shown in:

$$\dot{I}_{01}'' = \frac{\dot{I}_i \left(Y_{A1} + Y_{B1} + Y_{C1} \right)}{\left(Y_N + Y_A + Y_B + Y_C + g_f \right)} \tag{11}$$

$$\dot{I}_{0n}'' = \frac{\dot{I}_i \left(Y_{An} + Y_{Bn} + Y_{Cn} + g_f \right)}{\left(Y_N + Y_A + Y_B + Y_C + g_f \right)} \tag{12}$$

The fault current $\dot{I}_f''$ can be written as:

$$\dot{I}_f'' = \frac{g_f \dot{I}_i}{\left(Y_N + Y_A + Y_B + Y_C + g_f \right)} \tag{13}$$

The neutral voltage under the action of the active inverter injection device after the distribution network fault $\dot{U}_0$ can be written as :

$$\dot{U}_0 = \frac{\dot{I}_i}{\left(Y_N + Y_A + Y_B + Y_C + g_f \right)} - \frac{\dot{E}_A Y_A + \dot{E}_B Y_B + \dot{E}_C \left(Y_C + g_f \right)}{Y_A + Y_B + Y_C + g_f + Y_N} \tag{14}$$

The zero-sequence currents of healthy feeder $\dot{I}_{01}$ and faulty feeder $\dot{I}_{0n}$ are shown in:

$$\dot{I}_{01} = \dot{E}_A Y_{A1} + \dot{E}_B Y_{B1} + \dot{E}_C Y_{C1} + \dot{U}_0 \left(Y_{A1} + Y_{B1} + Y_{C1} \right) \tag{15}$$

$$\dot{I}_{0n} = \dot{E}_A Y_{An} + \dot{E}_B Y_{Bn} + \dot{E}_C \left(Y_{Cn} + g_f \right) + \dot{U}_0 \left(Y_{An} + Y_{Bn} + Y_{Cn} + g_f \right) \tag{16}$$

$\dot{K}_1$ and $\dot{K}_n$ are the asymmetry of feeder 1 and feeder n, respectively:

$$\dot{K}_1 = \frac{a^2 Y_{A1} + a Y_{B1} + Y_{C1}}{Y_{A1} + Y_{B1} + Y_{C1}} \tag{17}$$

$$\dot{K}_n = \frac{a^2 Y_{An} + a Y_{Bn} + Y_{Cn}}{Y_{An} + Y_{Bn} + Y_{Cn}} \tag{18}$$

The fault current $\dot{I}_f$ can be written as:

$$\dot{I}_f = \left(\dot{U}_0 + \dot{E}_C \right) g_f \tag{19}$$

The zero-sequence currents of healthy feeder $\dot{I}_{01}$ and faulty feeder $\dot{I}_{0n}$ can be written as:

$$\dot{I}_{01} = \left(\dot{K}_1 \dot{E}_C + \dot{U}_0 \right) \left(Y_{A1} + Y_{B1} + Y_{C1} \right) \tag{20}$$

$$\dot{I}_{0n} = \left(\dot{K}_n \dot{E}_C + \dot{U}_0 \right) \left(Y_{An} + Y_{Bn} + Y_{Cn} \right) + \dot{I}_f \tag{21}$$

From Eq. (14) to Eq. (16), flexible and active intervention of distribution network $\dot{U}_0$ and feeder zero-sequence currents can be implemented by injecting currents into the neutral point.

B.   High-Impedance Fault Detection and Faulty Feeder Selection Principle Independent of Distribution Network Parameters

The template is used to format your paper and style the text. All margins, column widths, line spaces, and text fonts are prescribed; please do not alter them. You may note peculiarities. For example, the head margin in this template measures proportionately more than is customary. This measurement and others are deliberate, using specifications

that anticipate your paper as one part of the entire proceedings, and not as an independent document. Please do not revise any of the current designations.

i. Principle of high-impedance fault detection based on the amount of injection current variation

From Eq. (14) to Eq. (19), when $\dot{U}_0$ is regulated to 0 by the active inverter injection device , the injection current $\dot{I}_i$ and fault current $\dot{I}_f$ are shown in:

$$\dot{I}_i = \dot{E}_A Y_A + \dot{E}_B Y_B + \dot{E}_C Y_C + \dot{E}_C g_f \tag{22}$$

$$\dot{I}_f = \dot{E}_C g_f \tag{23}$$

If there is no fault in the distribution network, the injection current when $\dot{U}_0$ is controlled to 0 by the active inverter injection device, and the zero-sequence currents in healthy feeder and faulty feeder n is shown in:

$$\dot{I}_{i-b} = \dot{E}_A Y_A + \dot{E}_B Y_B + \dot{E}_C Y_C \tag{24}$$

Eq. (24) represents the current generated in the distribution network due to three-phase asymmetry, which is not affected by the $\dot{U}_0$ and has a small amplitude. From (22), this current still exists during faults and its value is the inherent zero-sequence current. The current is affected by the degree of asymmetry of the three-phase ground conductor, and the amount of change is not significant. Subtract Eq. (22) and Eq. (24) to obtain the amount of change $\Delta\dot{I}_i$ in the injected current after the fault as shown in:

$$\Delta\dot{I}_i = \dot{E}_C g_f \tag{25}$$

As can be shown in Eq. (25), the injected current also changes due to the addition of the ground conductance branch in the fault phase, and $\Delta\dot{I}_i$ is only related to the fault conductance. In addition, the phase angle of $\Delta\dot{I}_i$ agrees with the phase angle of $\dot{E}_C$. Its value is the product of $\dot{E}_C$ and g_f .

Therefore, it is possible to monitor $\Delta\dot{I}_i$ to achieve the detection of faults. When ΔI_i exceeds a set threshold, it can be judged that a single-phase ground fault has occurred in the system. This detection method is not affected by parameters such as capacitive current and three-phase asymmetry of the distribution network. The fault detection criterion that is not affected by distribution network parameters is shown:

$$\Delta I_i > \lambda \tag{26}$$

Where λ is the threshold of the dynamic detection criterion for ground faults, the specific values of which are discussed in the subsequent section.

ii. Protection principle for detecting high impedance faulty feeder based on zero-sequence current magnitude

From Eq. (15) and Eq. (16), $\dot{I}_{0n}$ consists of three components. $\dot{I}_{0i}$ consists of only two components. They are the inherent zero-sequence current due to the asymmetry of the three-phase ground conductor and the component generated by the feeder-to-ground conductor under the action of $\dot{U}_0$. It can be shown that the difference between $\dot{I}_{0n}$ and $\dot{I}_{0i}$ is mainly attributed to the fault current. Faulty feeder selection requires accurate detection of the difference between the healthy feeder and the faulty feeder caused by fault currents, so faulty feeder selection needs to amplify the difference caused by fault currents.

As can be shown by the expressions for the components in the zero-sequence current, the inherent zero-sequence current is independent of the $\dot{U}_0$. The amplitude of the zero-sequence current component generated by the phase-to-ground conductor under the action of $\dot{U}_0$ varies linearly with the U_0. The fault current amplitude is linearly related to the fault phase voltage amplitude. When the control $\dot{U}_0$ is 0, the zero-sequence current component generated by the feeder-to-ground conductor under the action of the $\dot{U}_0$ is 0. The zero-sequence current of faulty feeder $\dot{I}_{0n}$ and healthy feeder $\dot{I}_{0i}$ is:

$$\dot{I}_{0n} = \dot{E}_A Y_{An} + \dot{E}_B Y_{Bn} + \dot{E}_C Y_{Cn} + \dot{E}_C g_f \tag{27}$$

$$\dot{I}_{01} = \dot{E}_A Y_{A1} + \dot{E}_B Y_{B1} + \dot{E}_C Y_{C1} \tag{28}$$

From Eq. (27) and Eq. (28), it can be shown that $\dot{I}_{0i}$ after adjusting the $\dot{U}_0$ to 0 is the feeder inherent zero-sequence current, and its amplitude is very small. $\dot{I}_{0n}$ is the vector sum of the feeder inherent zero-sequence current and fault current. The fault current is the product of the fault conductance with the fault phase-to-ground voltage. The fault current after adjusting the $\dot{U}_0$ to 0 is also increased, increasing the zero-sequence current amplitude difference characteristic of the healthy feeder and the faulty feeder. This enables HIF detection: when a ground fault is detected, the zero-sequence current amplitude of each feeder is compared, and the feeder with the largest amplitude is the faulty feeder. The SPG detection criteria as shown :

$$K_n = \frac{I_{0n}}{\max\left\{I_{01}, \cdots, I_{0n}\right\}} = 1 \tag{29}$$

Where: K_n is the ratio of the zero-sequence current of feeder n to the maximum value of the zero-sequence current in all feeders; the effective value of the zero-sequence current of feeder n is I_{0n}.

C. Analysis of factors affecting fault detection

Inputting or removing one feeder during normal operation of the distribution network changes the ground conductance of the three phases of the distribution network and causes a change in the injected current:

$$\Delta \dot{I}_i = \pm \left(\dot{E}_A Y_{Ai} + \dot{E}_B Y_{Bi} + \dot{E}_C Y_{Ci} \right) \tag{30}$$

Where: Y_{Ai}、Y_{Bi}、Y_{Ci} indicate the three-phase ground conductance of the feeder I, respectively. Take "+" when inputting the feeder and "-" when removing the feeder.

Distribution network feeders are divided into two types: overhead lines and cable lines. For cable lines, the degree of asymmetry is equal to 0 because the core of each phase is in a balanced position to the grounded cable metal sheath [17]. From Eq. (19), it can be shown that the amount of injected current change when casting and cutting the cable feeder is 0, which will not affect the dynamic detection of HIF.

The asymmetry of the overhead feeder generally does not exceed 3.5% [22]. The State Grid's Technical Guidelines for Distribution Network Planning and Design (DL/T 5729-2016) stipulates that the length of the distribution network feeder is less than 20km, and the overhead feeder pair capacitance is about 0.05uF/km [23]. At this time, the maximum variation of injected current when the 10kV distribution network is casting the overhead feeder is:

$$\Delta I_{i\max} = \left| \dot{E}_A Y_{Ai} + \dot{E}_B Y_{Bi} + \dot{E}_C Y_{Ci} \right| = \left| \dot{E}_A Y_{\Sigma i} \dot{K}_i \right| \le 3.5\% \times 20 \times 3 E_A \omega C_0 \sqrt{1 + d_{\max}^2} = 0.19\text{A} \tag{31}$$

$$\dot{K}_i = \frac{\left(Y_{Ci} + a Y_{Bi} + a^2 Y_{Ai} \right)}{Y_{Ai} + Y_{Bi} + Y_{Ci}} \tag{32}$$

Where $\dot{K}_i$ denotes the asymmetry of the feeder i. $d_{\max}$ denotes the maximum damping rate of the normal feeder, here taken as 0.1.

From Eq. (22), it can be shown that the maximum amount of injected current variation is 0.19A when the feeder of the 10kV distribution network is casting cut. According to Eq. (25), the amount of injected current variation when a 5kΩ HIF occurs in the 10kV distribution network is about 1.2A, which is much higher than the variation of injected current caused by feeder casting and cutting. Therefore, the influence of feeder casting on fault detection is also negligible through the appropriate selection of the fault detection rectification value.

Comprehensively analysing the factors affecting the reliability of the protection, the maximum variation of the injected current caused by switching the feeder, i.e., $\lambda < 0.19\text{A}$ should be evaded when adjusting the startup criterion of the ground-fault protection. Theoretically, when λ is set to any value greater than 0.19A, the proposed dynamic detection method will not judge the non-fault situation that causes the injection current change as a HIF. Thus, reliable dynamic detection of HIF can be implemented.

D.   HIF Handling Procedure

Existing fault detection and fault feeder selection protection methods are usually capable of detecting low-resistance ground faults with a fault resistance of 1kΩ or less. Therefore, the fault detection and fault feeder selection protection methods proposed in this chapter are mainly for HIF above 1kΩ. It can ensure that the fault current will not exceed the regulations and also maximize the fault detection and fault feeder selection capability of the distribution network.
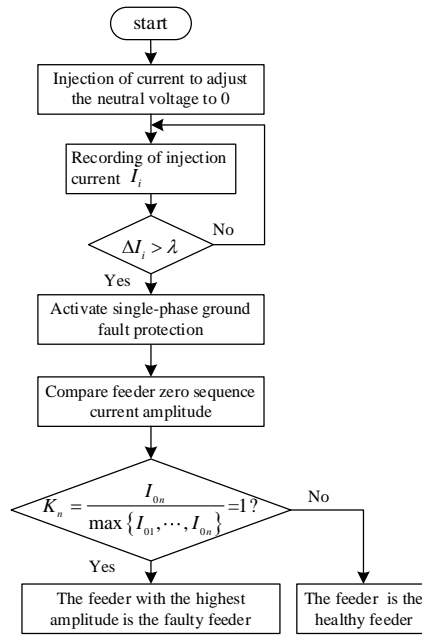
Figure 6: Implementation flow of HIF detection and faulty feeder selection protection method independent of distribution network parameters

The implementation flow of the protection method for HIF detection and faulty feeder selection independent of distribution network parameters is shown in Fig. 6. The implementation process is as follows: during normal operation of the distribution network, the $\dot{U}_0$ is controlled to 0, and the real-time monitoring of the injected current variation RMS value ΔI_i. If $\Delta I_i > \lambda$, then the system is judged to be faulty, and single-phase ground fault protection is activated. Compare the feeder zero-sequence current amplitude for fault feeder selection. And end the process after removing the faulty feeder.

IV.   SIMULATION ANALYSIS

The 10kV distribution network model shown in Fig. 7 is built in the PSCAD/EMTDC simulation. The HIF detection and faulty feeder selection method proposed in this chapter, which is not affected by the distribution network parameters, is simulated and verified. The distribution network model contains four feeders. The feeder simulation parameters are shown in Tab. 3, with a system detuning of -15% and an arc-suppression coil inductance of 0.207H.
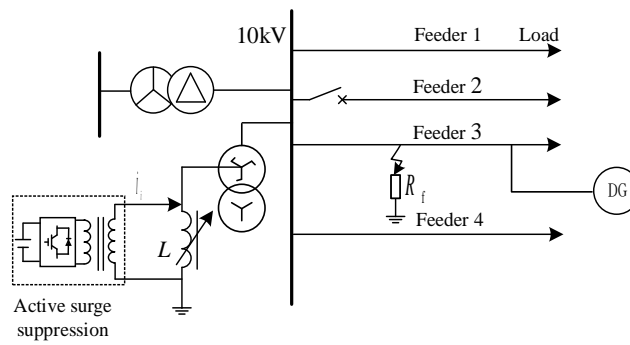
Figure 7: Topology of the simulation system

Table 3: Feeder simulation parameters

Parameters		Feeder1	Feeder2	Feeder3	Feeder4
	Phase A	6.23	0.52	0.41	3.90
C/ (μF)	Phase B	6.23	0.48	0.42	3.90
	Phase C	6.23	0.53	0.43	3.90
	Phase A	25547	204040	323490	27206
R/(Ω)	Phase B	25547	249650	301340	27206
	Phase C	25547	223570	323340	27206

A.   Ground Fault Dynamic detection

Set the integer value of the dynamic detection criterion $\lambda=0.2A$, and the fault occurs at 0.04s. When a 300Ω SPG fault occurs in phase C of feeder 3, the waveforms of the injected current and fault current are shown in Fig. 8.
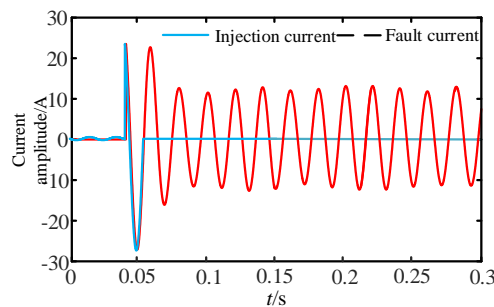
Figure 8: Injection and fault current waveforms

Before 0.04s $\dot{U}_0$ is regulated to 0, and the injected current is about 0.01 A. After the fault occurs, due to the variation of the asymmetry degree, the waveform of the injected current changes accordingly. As shown in Fig. 8, at this time the injected current is consistent with the fault current waveform, and the amount of change in the injected current is more than 10A, it is judged that SPG occurs.

When phase A of feeder 3 is grounded via 8kΩ, the RMS voltage of the conventional distribution network is shown in Fig. 9. The maximum post-fault $\dot{U}_0$ is 776V, which is less than 15% of the phase voltage (866V). Therefore, traditional fault detection methods fail to accurately sense the occurrence of a SPG. The fault will remain until the fault resistance falls to within detectable limits before it is sensed and faulted. Moreover, with the increase of cable lines and the expansion of the distribution network, the ability of traditional methods to detect HIF gradually decreases.
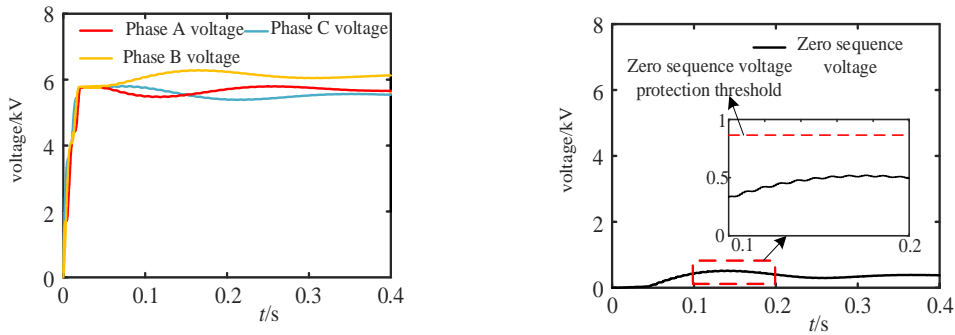
Figure 9: RMS voltage of 8kΩ single-phase ground fault system of conventional distribution network

Observing the three-phase voltage RMS, the C-phase voltage is about 5.8 kV after steady state, which is greater than the phase electromotive force and the B-phase voltage. This is because as the fault resistance increases, the effect of feeder asymmetry on the $\dot{U}_0$ gradually emerges and is even greater than the effect of fault resistance on the $\dot{U}_0$. The conclusion that the faulty phase voltage is less than the phase electromotive force will no longer apply.

The traditional phase selection method of taking the phase with the smallest voltage amplitude as the faulty phase cannot select the phase accurately. At this time, the ground fault processing method premised on the accurate identification of the faulty phase may even lead to changes in the properties of the fault [24-26].

The proposed fault dynamic detection method in this chapter is validated. The RMS values of the injected current variations are shown in Fig. 10 when phase C of feeder 3 is grounded via 3kΩ, 8kΩ and 10kΩ.
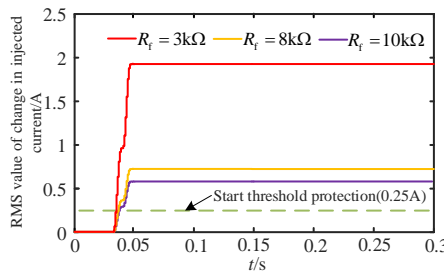
Figure 10: Variation of injected current for HIF

As can be shown in Fig. 10, the RMS value of the injected current variation decreases as the fault resistance increases. When the fault resistance is 10kΩ, it is about 0.57A, which is still greater than the integrating value of the ground fault detection criterion, and can realize the fault detection. Compared with the traditional fault detection criterion method, the fault dynamic detection method proposed in this chapter is not affected by the total conductance of the system.

The ground fault detection results when phase C of feeder 3 is grounded via different fault resistors are shown in Tab. 4.

Table 4: Dynamic fault detection results under different conditions

Prerequisite	ΔI_i (A)	Start-up results
$R_f = 300\Omega$	>10	activate
$R_f = 700\Omega$	8.24	activate
$R_f = 1k\Omega$	5.78	activate
$R_f = 3k\Omega$	1.93	activate
$R_f = 8k\Omega$	0.73	activate
$R_f = 10k\Omega$	0.59	activate
$R_f = 15k\Omega$	0.39	activate
Feeder 2 casting	0.08	non-activation

Tab. 4 shows that the proposed ground fault dynamic detection methods can properly determine the occurrence of HIF under different fault resistances.

B.   HIF faulty feeder selection

Without regulate $\dot{U}_0$, when a 5kΩ HIF occurs in feeder 3, the RMS zero-sequence current and phase angle of each feeder are shown in Fig. 11. Among them, $\dot{U}_0$ phase angle is 17.16°, and the information of each feeder after steady state is shown in Tab. 5.
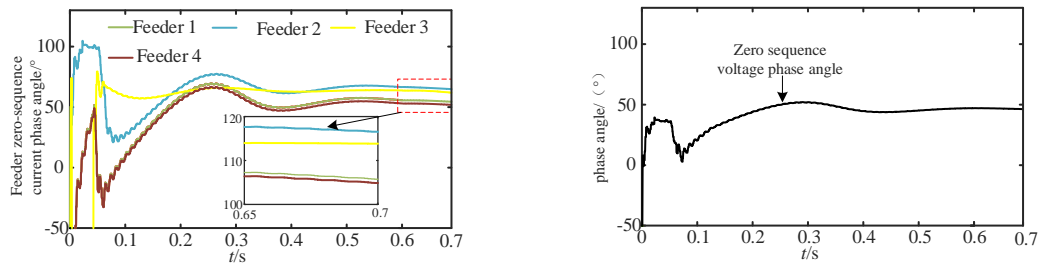
(a) Phase angle of zero-sequence current and phase angle of zero-sequence voltage of each feeder
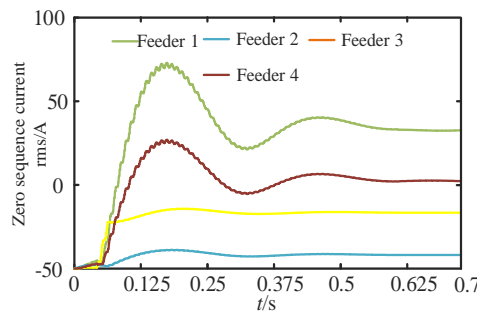
(b) Zero-sequence current RMS value for each feeder

Figure 11: Zero-sequence current and zero-sequence voltage variation curves of the feeder when R_f =5k Ω

Table 5: faulty feeder selection results when R_f **=5k Ω**

Feeder	zero-sequence current		active current method		zero-sequence admittance method	
	effective value(A)	phase angle(°)	effective value(A)	Faulty feeder detection results	phase angle(°)	Faulty feeder detection results
Feeder1	3.33	105.71	1.80	Faulty	88.48	healthy
Feeder2	0.33	116.55	0.12	healthy	99.32	Faulty
Feeder3	1.34	113.83	1.01	healthy	96.60	Faulty
Feeder4	2.08	105.13	1.97	healthy	87.90	healthy
Feeder5	1.64	105.40	1.63	healthy	88.17	healthy

As can be seen from Fig. 11 and Tab. 5, when a 5 kΩ HIF occurs in feeder 3, the phase angles of the zero-sequence currents in Feeder 1, Feeder 4, and Feeder 5 are approximately equal at 105.39°. The zero-sequence current phase angles of feeder 2 and feeder 3 are 116.07° and 113.64°, respectively. The zero-sequence conductance vectors are all within the fault region of the zero-sequence conductance of the resonant grounding system. At this time, the traditional faulty feeder selection method based on the zero-sequence conductor phase angle will judge that both feeder 2 and feeder 3 are faulty feeders. Moreover, since the zero-sequence active current of feeder 1 is the greatest, the faulty feeder selection method using the active current component will also incorrectly judge that feeder 1 is faulty.

In the feeder 1 and feeder 3 were set 700Ω, 1kΩ, 3kΩ, 5kΩ, 6kΩ SPG and arcing ground faults proposed in this chapter to verify the fault feeder selection method. When feeder 3 occurs 5kΩ HIF and arcing ground fault, the zero-sequence current of each feeder is shown in Fig. 12.

(a) Zero-sequence current waveforms of each feeder during 5kΩ HIF

(b) Zero-sequence current waveforms of each feeder during arcing ground faults
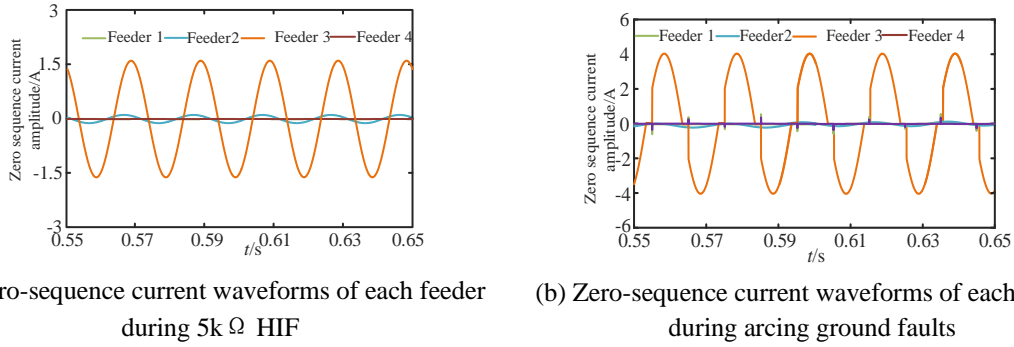
Figure 12: Zero-sequence current waveform of each feeder when a ground fault occurs on feeder 3

As can be shown in Fig. 12, before a fault occurs, the three-phase ground conductance of feeder 2 and feeder 3 are not exactly equal because the three-phase ground conductance of feeder 2 and feeder 3 are not exactly equal. Therefore, the feeder zero-sequence current is not zero, which is consistent with the conclusion of Eq. (28). After a fault occurs, the faulty feeder zero-sequence current increases significantly, while the healthy feeder does not change due to the feeder-to-ground conductance. Therefore, the zero-sequence current remains constant, and the zero-sequence currents of the faulty feeder and the healthy feeder are significantly differentiated. By comparing the amount of variation in the zero-sequence current of each feeder，it is possible to accurately identify the faulty feeder as feeder 3.

The faulty feeder selection results when Feeder 1 and Feeder 3 are grounded by different fault resistance are shown in Tab. 6.

Table 6: Faulty feeder selection results

Fault information		Feeder Information				Faulty feeder detection results
Faulty feeder	R_f (kΩ)	I_{01} (A)	I_{02} (A)	I_{03} (A)	I_{04} (A)	
Feeder 1	0.7	8.23	0.08	0.03	0.01	Feeder1
	1	5.77	0.08	0.03	0.01	Feeder1
	3	1.92	0.08	0.03	0.01	Feeder1
	5	1.15	0.08	0.03	0.01	Feeder1
	6	0.96	0.08	0.03	0.01	/
	arcing ground fault	2.78	0.08	0.03	0.0	Feeder1
Feeder 3	0.7	0.01	0.07	8.22	0.01	Feeder3
	1	0.01	0.07	5.75	0.01	Feeder3
	3	0.01	0.07	1.91	0.01	Feeder3
	5	0.01	0.07	1.14	0.01	Feeder3
	6	0.01	0.07	0.96	0.01	/
	arcing ground fault	0.00	0.08	2.78	0.00	Feeder3

In Tab. 6, when HIF occur on different feeders via the same fault resistance, the healthy feeder zero-sequence currents are all the inherent zero-sequence currents of the feeders, with extremely tiny amplitudes. The fault current is significantly greater than the inherent zero-sequence current, and the zero-sequence current amplitude of the faulted feeder is also greater than the zero-sequence current amplitude of all healthy feeders, which amplifies the fault characteristics. Using the faulty feeder selection criterion, the ratio of the zero-sequence current of the feeder to the maximum value of zero-sequence current among all feeders is calculated. The calculation results for faulty feeders are all 1, and the calculation results for healthy feeders are all 0. Faulty feeders can be accurately selected using the faulty feeder selection method proposed in this chapter.

V. CONCLUSION

This paper proposes a novel method for HIF protection in resonant grounding distribution networks with distributed power sources. Unlike existing approaches, the method remains unaffected by distribution network parameters. Before the occurrence of an HIF in the distribution network, the zero-sequence voltage is controlled to zero. Real-time monitoring of the change in injected current allows the construction of a dynamic fault detection criterion. By regulating the system's zero-sequence voltage to increase the zero-sequence current difference between the faulty

feeder and the healthy feeder, the zero-sequence current amplitude characteristics are used to effectively identify the faulty feeder. Finally, the feasibility of the proposed method is verified in PSCAD/EMTDC simulation, and the following conclusions are obtained:

1) The fault detection ability of the proposed method is not affected by parameters such as the capacitance current and three-phase asymmetry of the distribution network. It can effectively address the problem of decreased fault detection ability caused by the increase in the total capacitance of the distribution network to the ground due to the rise in the number of distribution network feeders and the proportion of cable feeders.

2) The primary reason for the failure of the traditional faulty feeder selection method under HIF conditions is that the fault impedance is significantly larger than the total impedance to the ground. The influence of the fault impedance on the three-phase voltage and feeder zero-sequence current is less pronounced than the impact of three-phase asymmetry on these parameters.

3) The proposed faulty feeder selection method demonstrates clear recognition of the faulty feeder. By adjusting the zero-sequence voltage, the difference in fault characteristics between the faulty feeder and the healthy feeder is increased. A faulty feeder selection criterion based on the zero-sequence current amplitude characteristics is constructed, eliminating the influence of ground parameter imbalance on faulty feeder selection. As a result, accurate faulty feeder selection for HIFs is achieved.

REFERENCES

[1] Wang X. W., Gao J, Wei X. X., et al. Faulty feeder detection under high impedance faults for resonant grounding distribution systems[J]. IEEE Transactions on Smart Grid, 2023, 14(3): 1880-1895.

[2] Liang L., Zhou Z., Qin H.J.J.O.E.S. An Improved Analysis of Distributed Resource Access Location and Capacity on Voltage Stability of Distribution Networks in Smart Grid [J]. 2024.

[3] Komrska T. , Peroutka Z. , Matuljak I. A novel least norm-based PWM for a four-leg earth fault compensator[C]// Proceedings of the 40th Annual Conference of the IEEE Industrial Electronics Society. Dallas : IEEE, 2014 : 1118-1123.

[4] Roy S., Suresh Babu P., Phanendra Babu N.V. A synchrophasor measurement-based fault locator with novel fault detection technique [J]. Journal of Electrical Systems, 2017, 13(3): 457-71.

[5] Jiang N. , Li S. C. , Wang L. , et al. A new method of measuring capacitance current in non-effective grounding power system[C]//International Conference on Condition Monitoring and Diagnosis IEEE. Xi'an, China : IEEE, 2016.

[6] Gonzalez C., Tant J., Germain J., et al. Directional, high-impedance fault detection in isolated neutral distribution grids[J]. IEEE Transactions on Power Delivery, 2018, 33(5): 2474-2483.

[7] Liu B. , Ma H. , Xu H. , et al. Single-phase-to-ground fault detection with distributed parameters analysis in non-direct grounded systems[J]. CSEE Journal of Power and Energy Systems, 2019.

[8] Guo M. F. , Zeng X. D. , Chen D. Y. , et al. Deeplearning-based earth fault detection using continuous wavelet transform and convolutional neural network in resonant grounding distribution systems[J]. IEEE Sensors Journal, 2018, 18(3) : 1291-1300

[9] Zeng H. , Yang P. H. , Cheng H. B. , et al. Research on single- phase to ground fault simulation base on a new type neutral point flexible grounding mode[J]. IEEE Access, 2019, 7 : 82563-82570.

[10] Shirkovets A. I. , Telegin A. V. , Kochura D. V. Conditions for effective ground fault suppression in distribution networks with capacitive current compensation[C] // 2016 Electric Power Quality and Supply Reliability (PQ), 2016, Tallinn, Estonia: 301-307.

[11] Janssen M. , Kraemer S. , Schmidt R. , et al. Residual current compensation (RCC) for resonant grounded transmission systems using high performance voltage source inverter[C]//Proceedings of 2003 IEEE PES Transmission and Distribution Conference and Exposition. Dallas : IEEE, 2003 : 574-578.

[12] Wang P. , Chen B. C. , Tian C. H. , et al. A novel neutral electromagnetic hybrid flexible grounding method in distribution networks[J]. IEEE Transactions on Power Delivery, 2017, 32(3) : 1350-1358.

[13] Liu K., Xiang G., Guo X., et al. Method for suppressing neutral point displacement overvoltage and suppression circuit in distribution network[C] // 2018 China International Conference on Electricity Distribution (CICED), September 17-19, 2018, Tianjin, China: 1726-1729.

[14] Amezua A. , Gutierrez I. , Pazos F. J. , et al . Active earthing system to optimise power quality in MV networks[C]//Proceedings of the 2007 9th International Conference on Electrical Power Quality and Utilisation. Barcelona : IEEE, 2007 : 1-6.

[15] Komrska T. , Peroutka Z. , Matuljak I. A novel least norm-based PWM for a four-leg earth fault compensator[C]// Proceedings of the 40th Annual Conference of the IEEE Industrial Electronics Society. Dallas : IEEE, 2014 : 1118-1123.

[16] Smirnov P. , Petzoldt J. , Kharitonov S. Control algorithm for an active ground fault current compensator in ungrounded distribution networks[C]//Proceedings of the 2018 20th European Conference on Power Electronics and Applications．Riga：IEEE，2018.

[17] Jia C. X., Wang C. L., Du G. F. Residual current compensation for single-phase grounding fault in coal mine power network[J]. International Journal of Mining Science and Technology, 2014, 24(2): 213-218.

[18] Zhao J., Deng J. W., Hu C. W., et al. Analysis and application of trajectory of neutral point displacement voltage during single-phase grounding fault in asymmetrical power grid[J]. Automation of Electric Power Systems, 2019, 43(5): 159-173.

[19] Liu B. W., Wang C. L., Li X. B. Analysis and application of zero-sequence voltage of single-phase ground fault asymmetrical system[J]. Proceedings of the CSEE, 2014, 34(28): 4959-4967.

[20] Zeng X. J., Wang Y. Y., Xia Y. F., et al. Single-phase grounding fault protection with sampled current difference between phases for ineffectively earthed distribution systems[J]. Journal of Changsha University of Science & Technology: Natural Science, 2006, 3(3): 78-83.

[21] Li Z. X., Wang X., Wang P. F., et al. Line selection method based on the zero-sequence admittance angle difference of power frequency and characteristical frequency[J]. Power System Protection and Control, 2019, 47(12): 13-21.

[22] Lin H. X. Lectures on national standard of power quality lecture five standards of three-phase voltage unbalance[J]. Building Electricity, 2011, 30(10): 25-29.

[23] Wu Y. S., Zhang Z. H., Wang J., et al. Engineering calculation method of single-phase grounding capacitance current in ungrounded neutral system[J]. Electrical Engineering, 2014(9): 108-111, 118.

[24] Wang W., Zeng X., Yan L. Principle and control design of active ground-fault arc suppression device for full compensation of ground current[J]. IEEE Transactions on Industrial Electronics, 2017, 64(6): 4561-4570.

[25] Ouyang S., Liu J., Yang Y., et al. Control strategy for arc-suppression-coil-grounded star-connected power electronic transformers[J]. IEEE Transactions on Power Electronics, 2019, 34(6): 5294-5311.

[26] Chen K., Zhang W., Xiao X. Faulted terminal open circuit voltage controller for arc suppression in distribution network[J]. IET Generation, Transmission & Distribution, 2020, 14(14): 2763-2770